# Deep Learning Framework for Precipitation Retrievals from Communication Satellites


Kumar Vijay Mishra

Kumar Vijay Mishra[1,2], Ahmad Gharanjik[1], M. R. Bhavani Shankar[1], and Björn Ottersten[1]

[1]*Interdisciplinary Centre for Security, Reliability and Trust (SnT), University of Luxembourg, Luxembourg*
[2]*IIHR - Hydroscience & Engineering, The University of Iowa, Iowa City, USA*
(Dated: 27 June 2018)

## 1. Introduction

It is well known that estimation of rainfall, while taking into account its spatio-temporal variability, is essential for several applications in earth sciences (Krajewski and Smith, 2002; Mishra et al., 2016). There is a rich heritage of research in analyzing multiple aspects of rainfall measurement and estimation using sensors such as rain gauges, disdrometers, weather radars and space-borne instruments (Testik and Gebremichael, 2013; Thurai et al., 2017). Over the past few decades, rainfall estimates based on weather radar measurements at low frequencies such as S-, C-, and X-bands have greatly enhanced our understanding of the precipitation structure. However, significantly large parts of the world, especially developing countries, remain uncovered from ground-based weather radar networks. Further, although radar-based precipitation estimates are increasingly used for quantitative precipitation estimation and forecast, it is also well established that these products suffer from large uncertainties (Mishra et al., 2013; Seo et al., 2015; Villarini and Krajewski, 2010). In regions where weather radars have been deployed, their large size and cost restricts the density of individual radar units to yield rainfall retrievals at high spatio-temporal resolutions (e.g. popular U.S. National Weather Service rainfall estimates are available at $\sim$ 1-4 km$^2$ resolution for a 14-minute volume scan) (Mishra et al., 2016; Thurai et al., 2017).

Recently, opportunistic use of communication satellite links to obtain valuable precipitation information in the regions that are beyond the coverage of conventional ground-based weather radars has garnered considerable research interest (Barthès and Mallet, 2013; Gharanjik et al., 2018a,b; Mugnai et al., 2015). Deployment of additional weather radars is expensive while there are overwhelmingly many ground satellite terminals spread across the world. The terminal link conditions, impacted heavily by attenuation in rain, are available at a central location (gateway station) in real-time making the entire setup usable in practice. The communication satellites also outnumber the spaceborne weather radars such as NASA's Tropical Rainfall Measurement Mission (TRMM) and Global Precipitation Measurement (GPM) (Hou et al., 2008).

Communication satellites operate at Ka-band where link signals suffer from strong attenuation in the rain medium (Mishra et al., 2012; Seto and Iguchi, 2015). Ground-based weather radars are typically not employed at millimeter wavelengths for estimating rainfall due to heavy signal attenuation. However, they are quite useful for observation of small hydrometeors such as clouds, drizzle and light snow as well as short-range rain rate retrievals (Chandra et al., 2015; Mishra, 2012). Additionally, Mie scattering effects at Ka-band may not be small causing the computation of scattering amplitudes difficult (Beard et al., 2010; Bringi et al., 2008; Nakamura et al., 2018). Nonetheless, at the locations where low-frequency weather radars may not be available, valuable but less accurate precipitation estimates have been obtained by Ka-band weather radars (Matrosov, 2005) and ground microwave links for cellular communication (Ostrometzky and Messer, 2018). The rainfall estimation procedure at Ka-band exploits the fact that both the rain rate $R$ and specific attenuation $A$ are approximately proportional to the 3.65th rain drop size distributions (DSD) moment at Ka-band (Matrosov et al., 2006) leading to a nearly linear relation between $R$ and $A$. It is also fortuitous that this relationship has relatively less, $\sim 10\%$, variability to temperature and DSD (Matrosov, 2005).

The carrier-to-noise-ratio (C/N) measurements (Gharanjik et al., 2018b) of the link are predominantly related to $A$ allowing derivation of $R$ estimates. However, the linear $R$-$A$ relation holds good only for heavy stratiform rain storms. In light rain, the attenuation is less significant and, consequently, difficult to estimate $A$. The $R$-$A$ linearity is also affected by the wind shear (Mittermaier et al., 2004) during convective storms. These various rainfall regimes are usually classified by the variability of radar measurables such as reflectivity, Doppler velocity, spectrum width, differential reflectivity, specific differential phase and copolar correlation coefficient that are estimated through advanced weather radar processing (Geerts and Dawei, 2004). The satellite user terminals (UT), on the other hand, are single-polarized passive receivers, and lack the ability to extract even the simplest parameters such as reflectivity and Doppler velocity which are necessary in order to differentiate between storm types and rainfall intensities. Despite these shortcomings, the presence of large number of satellite terminals is a motivation to exploit their measurements for rainfall estimation.

Due to the unavailability of radar-based products critical to correctly apply the $R$-$A$ algorithm, an alternative is to utilize learning methods which have the ability to extrapolate new features from a limited set of features contained in a training set (Lecun et al., 2015). Prior research (Orlandini and Morlini, 2000; Vulpiani et al., 2009) on S-, C-, X-, and Ku-band weather radars has adopted artificial neural network (ANN) for estimating rainfall wherein the difference between radar estimates and those obtained through *in situ* instruments such as rain gauges is used to train the network to adjust the radar relation parameters

until it converges on an optimal solution. We refer the reader to Testik and Gebremichael (2013) for an overview of these techniques that benefit from the availability of highly-parameterized data through the use of dual-polarization, high-resolution sampling and frequencies with minimal attenuation.

In contrast, our goal is to apply learning for rainfall estimation in a more information-limited setup from satellite communication signals. We first estimate $A$ by processing the received signal $C/N$ and then feed these estimates to a learning network to broadly classifies the storms based on their intensities so that the linear $R$-$A$ relationship can be appropriately exploited. Our previous work (Gharanjik et al., 2018a) has demonstrated the potential of Ka-band link for rainfall estimation by employing machine learning (ML) (Michalski et al., 2013) to classify dry and wet conditions. In Gharanjik et al. (2018b), we extended this work to enhance the retrieval performance by training the ML network to recognize dry, light and heavy rain regimes using data from the nearest weather radar and collocated rain gauges. Our analysis showed that our rain accumulations were in better agreement with the rain gauge than those from the nearest German weather service Deutscher Wetterdienst (DWD) radar. In comparison with the existing satellite link-based precipitation estimates obtained through conventional methods (Barthès and Mallet, 2013; Mugnai et al., 2015), our experimental set up comprises of broadband satellite systems that allow centralized rainfall estimation from gateway station.

In this work, we investigate deep learning (DL) (Lecun et al., 2015) in the specific context of rainfall estimation using the data from single-polarized passive receivers of ground terminals. The DL is a type of ML technique that works directly on the data rather than the user-defined data features and has been shown to provide state-of-the-art performance in a variety of applications (Elbir et al., 2018; Lecun et al., 2015). While classifying given $C/N$, it helps to look into the data before and after the present values. In this context, the recurrent neural networks (RNNs) (Medsker and Jain, 2001) are a class of DL architectures that are well suited to learn the time-dependent sequences of varying length. In this paper, specifically we use long short-term memory (LSTM) network (Hochreiter and Schmidhuber, 1997) - a type of RNN that is very efficient in exploiting dependencies over a long period of time and have been used successfully even on non-stationary data (Graves et al., 2005). Unlike our earlier work in Gharanjik et al. (2018b) which derived features such as mean and standard deviation of $C/N$ time series to input in an ML network for dry/wet classification, we directly use the $C/N$ series to train the LSTM. We aggregate the rainfall estimates from 35 UTs located in the Southwest Germany to generate an approximate rainfall map. We then compare our results with the observations from the nearest DWD radar in Southwest Germany. To the best of our knowledge, this is the first work that employs LSTM for the passive satellite links to generate rainfall estimates. Our initial results presented in this paper show reasonable accuracy wherein the 24-hour rain rate accumulations estimated by our proposed method has a difference of $1.8$ mm with that of the weather radar.

The paper is organized as follows. In the next section, we provide the details of the link setup and details of obtaining C/N parameter. In Section 3, we describe the DL technique to classify the data into dry/wet regions and aggregate estimates from all UTs to generate a rainfall map. The performance evaluation and comparison with DWD radar is detailed in Section 4 followed by concluding remarks in Section 5.

## 2. Communication Satellite Network

Broadband satellite systems offer bidirectional communications between the gateway (GW) stations and UTs enabling interactive satellite services (such as Internet provisioning), see Fig. 1. The link from the GW to UTs is called the forward (FWD) link and the link from UTs to the GW is the return (RTN) link.

### 2.1. System Description

In order to maintain a certain level of quality of service for users, GW stations continuously monitor the FWD and RTN links. The $C/N$ parameter measures quality of the communication link and received signals. The GW has access to end-to-end $C/N$ on both the links. However, we use only FWD links $C/N$ for rainfall estimation due to limitations in accessing RTN data. Average $C/N$ is available at the GW station every five minutes (average $C/N$ over five minutes) and stored in a database. It is generally assumed that the link between GW and the satellite (feeder link) is ideal. This is due to the fact that the transmit/receive antenna gain of the GW is very high. Therefore, the end-to-end $C/N$ is dominated by the $C/N$ of the user link (links between satellite and UTs). As a result, it can be assumed that variations of the end-to-end $C/N$ are mainly caused by the user links. The $C/N$ parameter is mainly affected by the rain attenuation at the operational Ka-band frequencies (broadband satellite) (Gharanjik et al., 2015). Therefore, there is a clear correlation between the $C/N$ variations and amount of the rainfall.

### 2.2. Experimental Set-up

In order to illustrate our proposed method, we have exploited the experimental system installed in Betzdorf, Luxembourg. The system includes a broadband satellite UT and a weather station equipped with rain gauge. The UT receives broadband

services from ASTRA 2F satellite located at the orbital position of 28.2 E. The links from satellite to UT operate at K-Band (19.70-20.20 GHz) while the links from UT to satellite is at Ka-Band (29.40-30.00 GHz). The elevation and azimuth angles of the links are 29.4° and 151.8°, respectively. We also used rainfall data from the C-band DWD weather radar (located in Southwest Germany) for studying the rain events over the satellite link. Fig. 2 depicts the relative locations of our set-up.

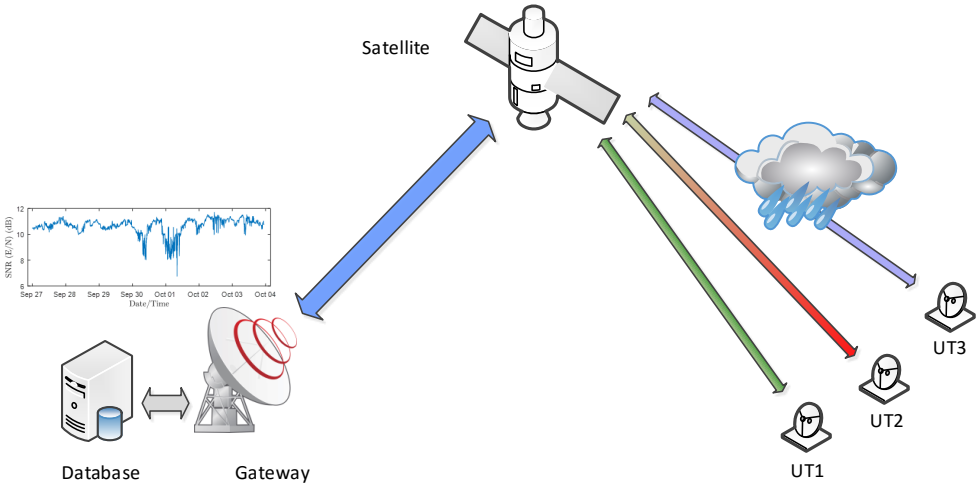


*Figure 1: Architecture of a Broadband Satellite Communication Systems. The $C/N$ data of the FWD and RTN links are collected by the gateway and stored at a database. We use these data for rainfall estimation.*

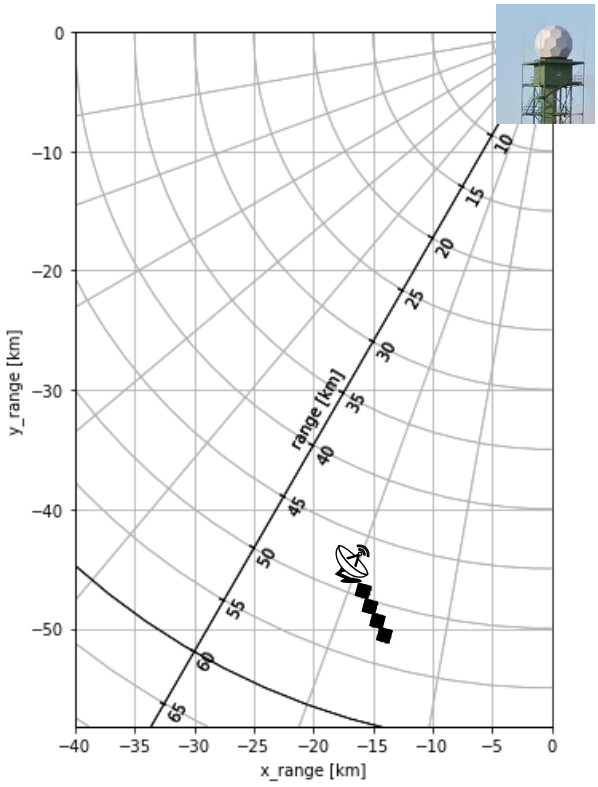


*Figure 2: Approximate projection of the satellite slant path on four radar bins shown by dark color. The first top left of these four black bins shows the location of the UT as well as the collocated rain gauge. The Southwest Germany DWD radar is about 50 km away from the UT.*

After training the rainfall estimation algorithm using the experimental set-up in Beztdorf, we applied it to $C/N$ data of 35 UTs. These UTs are distributed in 25 km $\times$ 20 km area in Southwest Germany. Fig. 3 shows the distribution and location of the 35 UTs in this region.

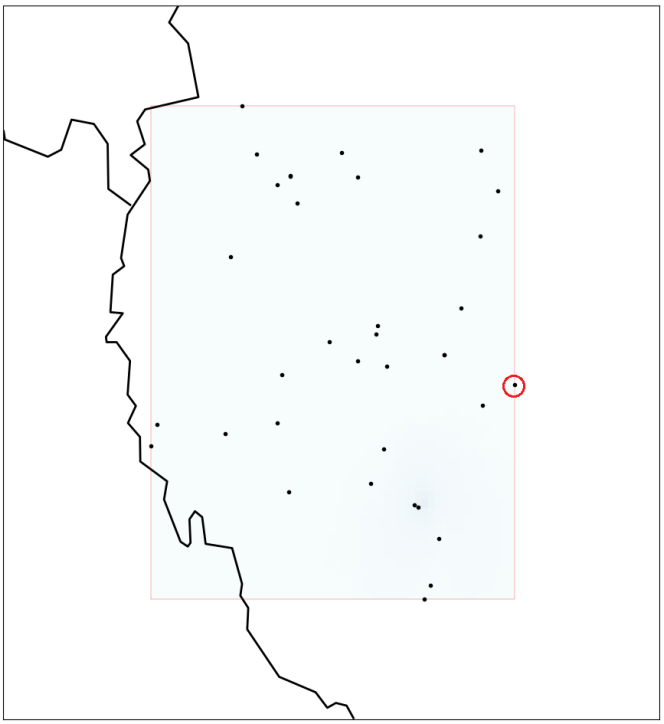

*Figure 3: Location of 35 satellite terminals in Southwest Germany (25km by 20km).*

### 2.3. Components of $C/N$

The first step towards estimating the rainfall from $C/N$ measurements is to determine the amount of signal attenuation caused by rainfall during the rain event. Central to this, is an understanding of the various components constituting the $C/N$ and the impact of rainfall on them. To this end, let us denote $C/N$ by $C(n)$, where $n$ is the index of measurement (data sample). Note that the data indexing starts from midnight and has a temporal resolution of 5 minutes, i.e., $n = 2$ represents 0005 UTC time of the first day of data collection.

Radio-wave propagation (and $C/N$) on Earth-Space links in millimeter wave frequencies is impacted by different tropospheric effects (Panagopoulos et al.), the major factor being the signal attenuation due to rain medium. We remark that co-channel interference also affects $C/N$. However, our set up does not employ multibeam coverage and frequency reuse. Consequently, the effect of co-channel interference is limited. Therefore, we assume that $C/N$ is only impacted by rain attenuation and can decompose $C/N$ (in dB) as,

$$C(n) = B(n) - D(n), \tag{2.1}$$

where, $B(n)$ is the baseline (reference level) that corresponds to the expected $C/N$ in dry (no-rain) situation assuming a fixed position. The $B(n)$ includes impact of gaseous absorption, cloud attenuation, scintillations and noise in the microwave link. The $D(n)$ accounts for attenuation in rain and is zero in dry situations.

## 3. Rainfall Estimation Algorithm

In this section, we detail the proposed rainfall estimation algorithm. It consists of two steps: rain regime classification and rain rate calculation. Classification is required to find the baseline and signal attenuation ($B(n)$ and $D(n)$, respectively). We calculate the rain rate using $D(n)$ as recommended by the ITU-R model (ITU, 2013, 2005).

### 3.1. Rainfall Classification: LSTM algorithm

The goal of the classification algorithm is to distinguish between two classes: rain and dry given the $C/N$ measurements. We consider LSTM here which is an RNN technique designed to efficiently find and infer long-range temporal dependencies in the time series. It was developed to counter the exponential blow-up or decay of the backpropagated error in existing RNNs leading to inaccessibility of long time lags.

The LSTM network can be considered as a sequence-to-label system. Its hidden layer consists of memory blocks which comprises of one or more recurrently connected memory cells and multiplicative units such as the input, output and forget gates. The latter three are the continuous analogues of write, read and reset operations for the memory cells. The network

interacts with the memory cells only via the gates. The cell input, network output and previous cell values are multiplied by the activation of the input, output and forget gate, respectively.

### 3.2. Rainfall Estimation: $R$-$A$ Relation

After identifying the rain and dry events, we use a procedure similar to the one discussed in (Gharanjik et al., 2018a) to estimate the signal attenuation due to rain, i.e., $D(n)$. The ITU recommends (ITU, 2013, 2005) following power-law relationship between the specific attenuation $A$ (dB/km) and rain rate $R$ (mm/h)

$$A = kR^{\alpha}, \tag{3.1}$$

where the coefficients $k$ and $\alpha$ depend on the frequency and polarization of the link. For the considered experimental setup at FWD link, we compute these values as follows: $k = 0.0939$ and $\alpha = 1.0199$. The specific attenuation is obtained as $A = D/L_s$ where $D$ is the signal attenuation defined in (2.1). Here, $L_s = 4.9276$ km is the slant path length of the satellite link (Gharanjik et al., 2018a).

### 3.3. Rainfall Map Generation

After converting the $C/N$ time-series to $R$, our objective is to generate a rainfall map for the region in Southwest Germany with 35 *in situ* UTs. We used the trained LSTM to estimate the rainfall rate for each UT. Thereafter, we applied inverse distance weighting (IDW) interpolation technique (Lu and Wong, 2008) create an approximate rainfall distribution over the entire region (see Fig. 3). The IDW assumes that the regions close to one another experience similar rain intensities than those that are farther apart. For each point on the map, we considered 5 closest neighboring UTs for computing the IDW weights.

## 4. Numerical Results

In this section, we present some numerical results for the proposed rainfall estimation approach. We employ an LSTM layer with 5 units and two outputs, each representing a class (dry or wet). Each LSTM unit looks back to the last 10 time steps in order to determine the class of the current $C/N$ value. The classification output layer consists of $y_1$ and $y_2$ that provide the probability of rain and dry events, respectively. Fig. 4 shows the architecture of the LSTM network. Here, we standardized the input data ($C/N$) (rescaling the data so that the mean of $C/N$ values is 0 and the standard deviation is 1) in order to speed-up the learning and convergence of the network.

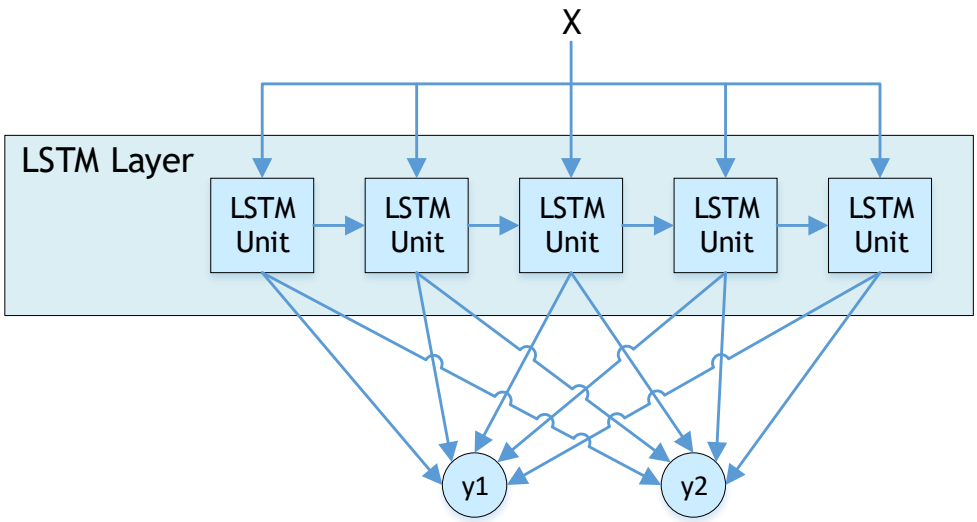


*Figure 4: Structure of LSTM network for rain/dry classification.*

All LSTM blocks had the following activation functions: logistic sigmoids in the range [-1, 1] for the input and output activation functions of the cell, and in the range [0, 1] for the forget gates. We used data from the set-up mentioned in Section 2 and partitioned them into LSTM training and test data. All nets were trained with gradient descent, using a learning rate of $10^{-1}$ and a momentum of 0.9. At the end of each iteration, the weights were updated and network activations were reset to zero. The output layers had softmax classifers, and the cross entropy objective function was used for training.

Following the procedure outlined in Section 3.2, we obtained estimates of $R$ for each UT. Fig. 5 shows rain rates and rain accumulations over 24 hour period from 1200 UTC on 22 May 2018 to 1200 UTC on 23 May 2018 as estimated by the Southwest Germany DWD radar (dashed blue line) and the satellite link UT (encircled terminal on Fig. 3) using our proposed algorithm (solid red line). The UT estimates follows the radar closely leading to a single-day accumulation difference of $\sim 1.5$ mm only.

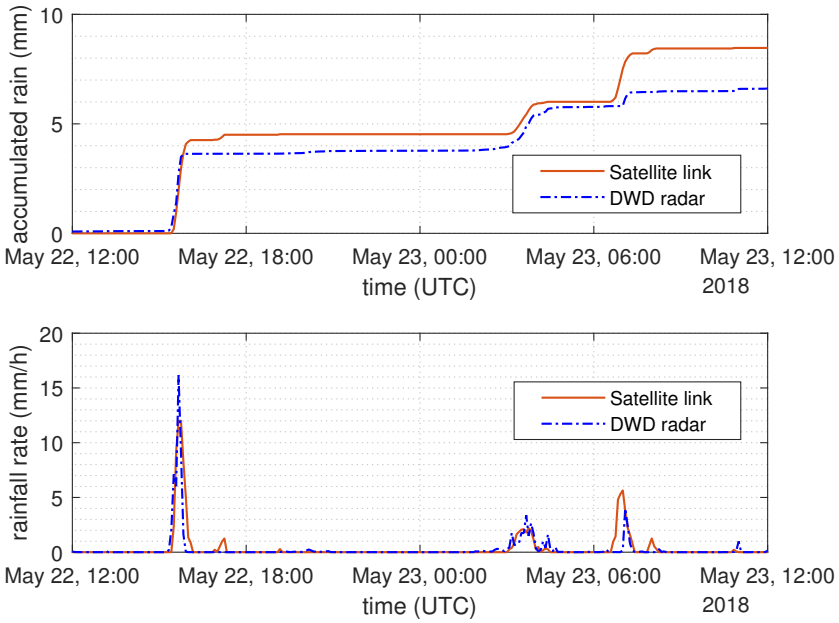


*Figure 5: Rain accumulations during 24 hours from 1200 UTC on 22 May 2018 till 1200 UTC on 23 May 2018 as observed by the Southwest Germany DWD radar (dashed blue line) and satellite link (encircled UT in Fig. 3) using our proposed algorithm (solid red line).*

Finally, Fig. 6 compares 5-minute accumulations of the Southwest Germany DWD radar with the rainfall distribution generated by LSTM-based UT estimates at two different time intervals for a passing storm on 22 May 2018 UTC. The two snapshots which are about 35 minutes apart show that UT estimates capture the general direction and locations of the storms as observed by the radar. Note that the location of the radar beam is higher than the ground while the estimates from the UTs are closer to the ground. Several other factors such as differences in resolutions and sampling rates enhance the dissimilarities between the two estimates. As we show in Gharanjik et al. (2018b), the UT estimates are improved by training with the rain gauge data wherever possible. Nonetheless, our study demonstrates that DL can be effectively used to obtain valuable estimates of rainfall from UTs in regions where radar coverage may be missing.

## 5. Summary

We proposed and investigated a DL framework for rainfall estimation based on opportunistic use of $C/N$ measurements from broadband satellite communication networks. The learning network was modeled after LSTM which searches and recognizes long-term temporal dependencies in time-series data. We trained LSTM to directly classify the $C/N$ data from the satellite links into dry and wet weather without using any user-defined data features. Thereafter, the events classified as rain storms were estimated for rain rates using the $R$-$A$ expression following the ITU-R recommendations. Our comparisons of the rainfall distribution map generated from LSTM-based UT estimates with the nearest weather radar shows that our algorithm captures the major features of the storm even though very limited information about the weather was available to the UT set-up. This study demonstrates that DL is a promising framework to extract valuable, although less accurate, precipitation retrievals via the communication satellite links. In future, our goal is to continue improving the UT estimates through use of other advanced DL techniques and better training data.

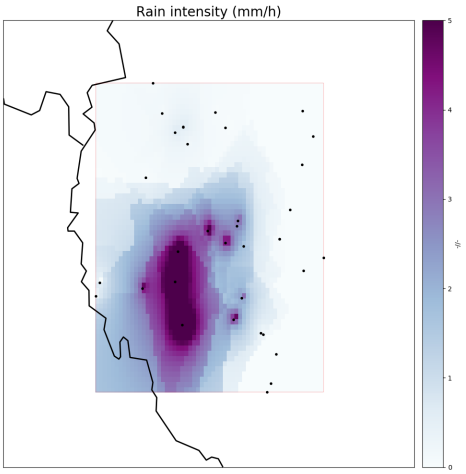


(a) Rainfall map (intensity) generated using $C/N$ data from 35 satellite terminals at 1500 UTC on 22 May 2018

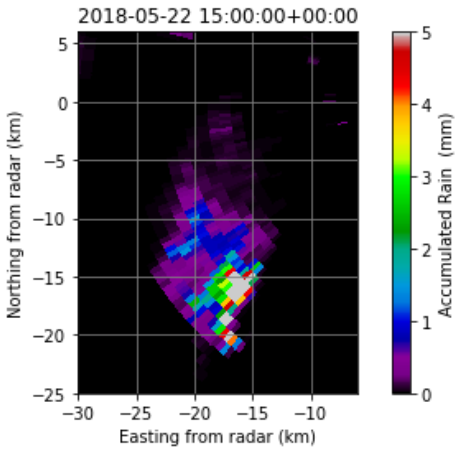


(b) Rainfall map (accumulation over 5 minutes) from DWD radar at 1500 UTC on 22 May 2018

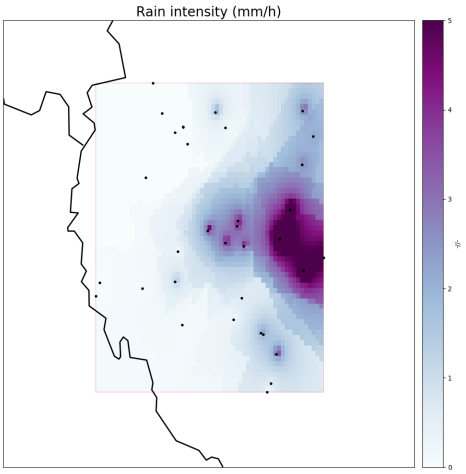


(c) Rainfall map (intensity) generated using $C/N$ data from 35 satellite terminals at 1535 UTC on 22 May 2018

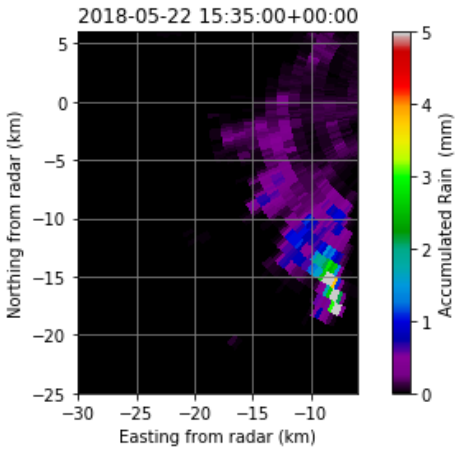


(d) Rainfall map (accumulation over 5 minutes) from DWD radar at 1535 UTC on 22 May 2018

*Figure 6: Comparison of the rainfall maps produced by our LSTM-based algorithm and the nearest DWD radar at two different intervals for a storm passing over Southwest Germany on* 22 *May* 2018 *UTC.*

**Acknowledgement**

This work was partially funded by the Luxembourg National Research Fund (FNR) for the Proof of Concept project RAFAEL bearing contract POC/17/ 11648950.

**References**

"Propagation data and prediction method required for the design of the Earth-space telecommunication systems," ITU-R Recommendation P.618-11, Geneva, Switzerland, Tech. Rep., 2013.

"Specific attenuation model for rain for use in prediction methods," ITU-R Recommendation P.838-3, Geneva, Switzerland, Tech. Rep., 2005.

L. Barthès and C. Mallet, "Rainfall measurement from opportunistic use of earth-space link in Ku band," *Atmospheric Measurement Techniques*, vol. 6, no. 8, pp. 2181–2193, 2013.

K. V. Beard, V. Bringi, and M. Thurai, "A new understanding of raindrop shape," *Atmospheric Research*, vol. 97, no. 4, pp. 396–415, 2010.

V. Bringi, M. Thurai, and D. Brunkow, "Measurements and inferences of raindrop canting angles," *Electronics Letters*, vol. 44, no. 24, pp. 1425–1426, 2008.

A. Chandra, C. Zhang, P. Kollias, S. Matrosov, and W. Szyrmer, "Automated rain rate estimates using the Ka-band ARM zenith radar (KAZR)," *Atmospheric Measurement Techniques*, vol. 8, no. 9, p. 3685, 2015.

A. M. Elbir, K. V. Mishra, and Y. C. Eldar, "Cognitive radar antenna selection via deep learning," *arXiv preprint arXiv:1802.09736*, 2018.

B. Geerts and Y. Dawei, "Classification and characterization of tropical precipitation based on high-resolution airborne vertical incidence radar. Part I: Classification," *Journal of Applied Meteorology*, vol. 43, no. 11, pp. 1554–1566, 2004.

A. Gharanjik, M. R. Bhavani Shankar, P.-D. Arapoglou, and B. Ottersten, "Multiple gateway transmit diversity in Q/V band feeder links," *IEEE Transactions on Communications*, vol. 63, no. 3, pp. 916–926, 2015.

A. Gharanjik, M. R. Bhavani Shankar, F. Zimmer, and B. Ottersten, "Centralized rainfall estimation using carrier-to-noise of satellite communication links," *IEEE Journal on Selected Areas in Communications*, 2018, in press.

A. Gharanjik, K. V. Mishra, M. R. Bhavani Shankar, and B. Ottersten, "Learning-based rainfall estimation via communication satellite links," in *IEEE Statistical Signal Processing Workshop*, 2018.

A. Graves, S. Fernández, and J. Schmidhuber, "Bidirectional LSTM networks for improved phoneme classification and recognition," in *International Conference on Artificial Neural Networks*, 2005, pp. 799–804.

S. Hochreiter and J. Schmidhuber, "Long short-term memory," *Neural computation*, vol. 9, no. 8, pp. 1735–1780, 1997.

A. Y. Hou, G. Skofronick-Jackson, C. D. Kummerow, and J. M. Shepherd, "Global precipitation measurement," in *Precipitation: Advances in Measurement, Estimation and Prediction*, S. C. Michaelides, Ed. Springer, 2008.

W. Krajewski and J. Smith, "Radar hydrology: Rainfall estimation," *Advances in Water Resources*, vol. 25, no. 8-12, pp. 1387–1394, 2002.

Y. Lecun, Y. Bengio, and G. Hinton, "Deep learning," *Nature*, vol. 521, no. 7553, pp. 436–444, 2015.

G. Y. Lu and D. W. Wong, "An adaptive inverse-distance weighting spatial interpolation technique," *Computers & geosciences*, vol. 34, no. 9, pp. 1044–1055, 2008.

S. Y. Matrosov, "Attenuation-based estimates of rainfall rates aloft with vertically pointing Ka-band radars," *Journal of Atmospheric and Oceanic Technology*, vol. 22, no. 1, pp. 43–54, 2005.

S. Y. Matrosov, P. T. May, and M. D. Shupe, "Rainfall profiling using atmospheric radiation measurement program vertically pointing 8-mm wavelength radars," *Journal of Atmospheric and Oceanic Technology*, vol. 23, no. 11, pp. 1478–1491, 2006.

L. Medsker and L. Jain, "Recurrent neural networks," *Design and Applications*, vol. 5, 2001.

R. S. Michalski, J. G. Carbonell, and T. M. Mitchell, *Machine learning: An artificial intelligence approach*. Springer Science & Business Media, 2013.

K. V. Mishra, "Frequency diversity wideband digital receiver and signal processor for solid-state dual-polarimetric weather radars," Master's thesis, Colorado State University, 2012.

K. V. Mishra, V. Chandrasekar, C. Nguyen, and M. Vega, "The signal processor system for the NASA dual-frequency dual-polarized Doppler radar," in *IEEE International Geoscience and Remote Sensing Symposium*, 2012, pp. 4774–4777.

K. V. Mishra, A. Kruger, and W. F. Krajewski, "Monitoring cross-channel correlation solar scan measurements using the Iowa X-band polarimetric radars," in *IEEE International Geoscience and Remote Sensing Symposium*, 2013, pp. 1688–1691.

K. V. Mishra, W. F. Krajewski, R. Goska, D. Ceynar, B.-C. Seo, A. Kruger, J. J. Niemeier, M. B. Galvez, M. Thurai, V. Bringi *et al.*, "Deployment and performance analyses of high-resolution Iowa XPOL radar system during the NASA IFloodS campaign," *Journal of Hydrometeorology*, vol. 17, no. 2, pp. 455–479, 2016.

M. P. Mittermaier, R. J. Hogan, and A. J. Illingworth, "Using mesoscale model winds for correcting wind-drift errors in radar estimates of surface rainfall," *Quarterly Journal of the Royal Meteorological Society*, vol. 130, no. 601, pp. 2105–2123, 2004.

C. Mugnai, F. Sermi, F. Cuccoli, and L. Facheris, "Rainfall estimation with a commercial tool for satellite internet in Ka band: Model evolution and results," in *IEEE International Geoscience and Remote Sensing Symposium*, 2015, pp. 890–893.

K. Nakamura, Y. Kaneko, K. Nakagawa, H. Hanado, and M. Nishikawa, "Measurement method for specific attenuation in the melting layer using a dual Ka-band radar system," *IEEE Transactions on Geoscience and Remote Sensing*, vol. 56, no. 6, pp. 3511–3519, 2018.

S. Orlandini and I. Morlini, "Artificial neural network estimation of rainfall intensity from radar observations," *Journal of Geophysical Research: Atmospheres*, vol. 105, no. D20, pp. 24 849–24 861, 2000.

J. Ostrometzky and H. Messer, "Dynamic determination of the baseline level in microwave links for rain monitoring from minimum attenuation values," *IEEE Journal of Selected Topics in Applied Earth Observations and Remote Sensing*, vol. 11, no. 1, pp. 24–33, 2018.

A. D. Panagopoulos, P.-D. M. Arapoglou, and P. G. Cottis, "Satellite communications at Ku, Ka, and V bands: Propagation impairments and mitigation techniques," *IEEE Communications Surveys and Tutorials*, vol. 6, no. 3, pp. 2–14.

B.-C. Seo, W. F. Krajewski, and K. V. Mishra, "Using the new dual-polarimetric capability of WSR-88D to eliminate anomalous propagation and wind turbine effects in radar-rainfall," *Atmospheric Research*, vol. 153, pp. 296–309, 2015.

S. Seto and T. Iguchi, "Intercomparison of attenuation correction methods for the GPM dual-frequency precipitation radar," *Journal of Atmospheric and Oceanic Technology*, vol. 32, no. 5, pp. 915–926, 2015.

F. Y. Testik and M. Gebremichael, *Rainfall: State of the science*. John Wiley & Sons, 2013, vol. 191.

M. Thurai, K. V. Mishra, V. Bringi, and W. F. Krajewski, "Initial results of a new composite-weighted algorithm for dual-polarized X-band rainfall estimation," *Journal of Hydrometeorology*, vol. 18, no. 4, pp. 1081–1100, 2017.

G. Villarini and W. F. Krajewski, "Review of the different sources of uncertainty in single polarization radar-based estimates of rainfall," *Surveys in Geophysics*, vol. 31, no. 1, pp. 107–129, 2010.

G. Vulpiani, S. Giangrande, and F. S. Marzano, "Rainfall estimation from polarimetric S-band radar measurements: Validation

of a neural network approach," *Journal of Applied Meteorology and Climatology*, vol. 48, no. 10, pp. 2022–2036, 2009.